

Model Predictive Current Control of Nine-Phase Open-End Winding PMSMs With an Online Virtual Vector Synthesis Strategy

Haifeng Wang[✉], Graduate Student Member, IEEE, Xinzhen Wu^{ID}, Xiaoqin Zheng^{ID}, Member, IEEE, and Xibo Yuan^{ID}, Senior Member, IEEE

Abstract—The current error is hard to avoid for finite control set model predictive current control (FCS-MPCC) in nine-phase open-end winding permanent magnet synchronous motors. To overcome this problem, an online virtual voltage vector (V^3) synthesis strategy is proposed in this article. First, a group of V^3 's without harmonic voltage components are designed as the basic vectors for online synthesis. Then, two adjacent basic V^3 's and a zero vector are used to synthesize a new V^3 , which can output arbitrary amplitude and phase angle in the fundamental space. The two basic V^3 's are directly selected from the located sector of the predicted reference voltage vector (RVV), and their duration ratio can be simply calculated according to the angle of the RVV in the sector. In this way, the zero error is realized between the new V^3 and RVV. Moreover, an online pulse generation algorithm corresponding to the new V^3 is proposed, which can calculate the symmetrical pulse sequences in real-time for the multiphase OW drive system without the space vector modulator. Finally, experimental results have verified the effectiveness and superiority of the proposed strategy, in comparison to existing FCS-MPCC in multiphase OW motor drive systems.

Index Terms—Model predictive control (MPC), nine-phase permanent magnet synchronous motors (PMSM), online synthesis, open-end winding, virtual vector, zero control error.

I. INTRODUCTION

OWING to a higher dc-link voltage utilization, control flexibility and fault tolerance, multiphase permanent magnet synchronous motors with open-end winding (OW-PMSMs) have been considered as promising candidates in high-power

Manuscript received 22 February 2022; revised 25 April 2022; accepted 29 April 2022. Date of publication 17 May 2022; date of current version 16 November 2022. This work was supported by the National Natural Science Foundation of China under Grant 52037005, Grant U2106217 and Grant 51907093. (Corresponding author: Xinzhen Wu.)

Haifeng Wang, Xinzhen Wu, and Xiaoqin Zheng are with the College of Electrical Engineering, Qingdao University, Qingdao 266071, China (e-mail: 2018010022@qdu.edu.cn; wuxinzhen@qdu.edu.cn; zhengxiaoqin@qdu.edu.cn).

Xibo Yuan is with the College of Electrical Engineering, Qingdao University, Qingdao 266071, China, and also with the Department of Electrical and Electronic Engineering, University of Bristol, BS8 1UB Bristol, U.K. (e-mail: xibo.yuan@bristol.ac.uk).

Color versions of one or more figures in this article are available at <https://doi.org/10.1109/TIE.2022.3174241>.

Digital Object Identifier 10.1109/TIE.2022.3174241

high-reliability electric propulsion applications [1]–[3]. In addition, finite control set model predictive control (FCS-MPC) has received great attention in multiphase motor drive systems thanks to the increasing computational capability of microprocessors [4]. Compared with conventional control strategies, such as field-oriented control and direct torque control, FCS-MPC has fast dynamic response and it is easy to include nonlinear constraints [5], [6]. Especially, for multivariable control in multiphase drives, FCS-MPC can be implemented simply without adding new controllers [7].

The classic FCS-MPC strategy evaluates all candidate voltage vectors through the predictive model, and selects the vector that makes the control variable closest to the reference value. Thus, the inverter is directly driven by applying the switching state corresponding to the optimal vector without an external modulator [8]. Among various kinds of FCS-MPC strategies, model predictive current control (MPCC) is one of the most popular and classical solutions in three-phase machine drives because the weighting factor is intrinsically absent. However, in multiphase drives, where multiple planes must be regulated at the same time, the weighting factor must be considered. Meanwhile, the discrete and single voltage vector output limits the improvement of operation performance. In particular, according to the extended vector space decomposition (VSD) theory, there are harmonic subspaces in the multiphase system, which introduces the low-order harmonic currents that cannot be neglected [9], [10]. Obviously, using only a single voltage vector during the whole control period cannot regulate all subspace components at the same time, and the control error always exists due to the discretization of voltage vector.

Aiming to eliminate the influence of voltage vector in harmonic subspaces, the virtual voltage vector (V^3) is proposed by the means of voltage vector synthesis [11]. In five- and six-phase PMSM drives, the V^3 is synthesized by two or more voltage vectors to obtain zero average amplitudes in the harmonic subspace [12], [13]. For the back electromotive force (EMF) odd harmonics created by nonsinusoidal flux, Xiong *et al.* [14] proposed the method that can simultaneously control the fundamental plane current and harmonic plane current in the five-phase PMSM, so the stator current harmonics can be suppressed effectively. Gonçalves *et al.* [15] presented a multistage predictive current control strategy, which contains fundamental and secondary control stages that are responsible for tracking the reference currents in both subspaces separately. However, the fixed amplitude of the V^3 deteriorates the steady-state performance. In addition, an observer-based predictive vector-resonant

control scheme is proposed in [16] to suppress periodic disturbances resulting from converter dead-time effect and rotor flux harmonics. In order to output the V^3 with flexible amplitude, Xue *et al.* [17] reported a FCS-MPCC scheme with optimal duty ratio, which combines the selected V^3 and zero vector in each control cycle. Besides, Saeed *et al.* [18] proposed a deadbeat FCS-MPCC with duty ratio. In this method, the deadbeat current control (DBCC) is introduced to obtain the reference voltage vector (RVV), and then the optimal V^3 is directly selected according to the located sector of the RVV. It not only improves the control accuracy with the duty ratio optimization, but also reduces the computational burden significantly. However, the control sets in the abovementioned methods are composed of the discrete voltage vectors calculated offline. Although the amplitude of the output vector is variable, the error between the output vector and RVV is still difficult to eliminate.

An effective way to reduce and eliminate the control error is to dynamically synthesize the V^3 in real time according to the control requirement [19], [20]. An online vector synthesis scheme is proposed in [21], which synthesizes multiple vectors in the sector where the RVV is located, and selects the optimal one as the output by the cost function. Nevertheless, the synthesized vector points are limited and unable to cover the whole synchronous space frame. In [22], a dynamic voltage vectors (DVV) strategy is proposed further. The V^3 are constantly changing to search for the optimal combination in each control cycle. However, the vector preselection and amplitude optimization processes are complicated with an increased computational burden. In [23], the smart voltage vector (SVV) is synthesized by three vectors to realize that the output vector covers the whole surface in $\alpha - \beta$ plane. However, the selection of three optimal vectors still requires a lot of online iterative search, and the optimal dwell time of each vector is searched in 12 discrete values according to the predefined interval. To remove the control error in FCS-MPCC, Zhao *et al.* [24] and Song *et al.* [25], respectively, proposed a continued modulation V^3 scheme without using a modulator for five-phase drive systems. In [24], a cascaded optimization procedure is introduced to determine the voltage vectors participating in the synthesis, the phase angle of the synthesized new V^3 , and the duty ratio. This optimization strategy requires two duty ratio calculations and two cost function exploration processes. In [25], the synthesis results of each set of adjacent V^3 's is evaluated, and then, the optimal new V^3 is realized by substituting the precalculated duty ratio into the dwell time calculation of each leg. Therefore, the repeated evaluation process cannot be absent. Also, in [26], the modulated MPC (M^2 PC) uses four active vectors to improve further the steady-state error of the stator currents tracking in $d - q$ plane. However, the modulation method is not applicable to open-end winding multiphase motors with H-bridge converters.

In nine-phase OW-PMSM drives, the online V^3 synthesis faces new challenges. First, more harmonic subspaces than five- and six-phase drives means that more voltage vectors need to participate in the synthesis. Then, different from star-connected motor drives, the synthesized vector is the result of the simultaneous action by the dual inverter. Consequently, it is a real challenge to generate the new pulse sequences online in the multiphase OW drives without using a space vector modulator, although some efforts on virtual vector output method have been made recently for multiphase machines [27]–[29]. Moreover, the computational burden needs to be further reduced to adapt to the complexity of the system.

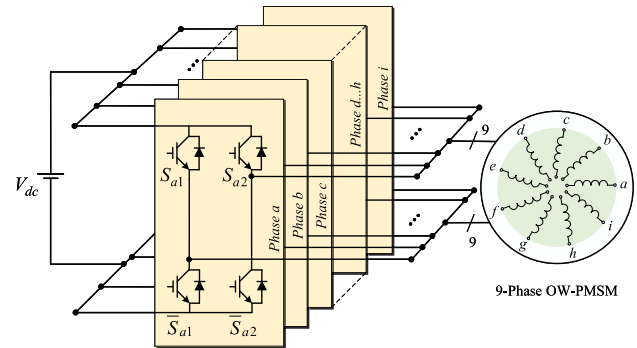


Fig. 1. Schematic of the nine-phase OW-PMSM drive system.

In this article, an online V^3 synthesis strategy-based FCS-MPCC for nine-phase OW-PMSMs is first proposed. The first objective is to establish the discrete basic V^3 set that can eliminate the voltage components in the harmonic subspaces. The second objective is to synthesize a new V^3 online using two adjacent V^3 's and a zero vector, so that the output V^3 covers any amplitude and phase angle in the whole fundamental subspace. The third objective is the online generation of the symmetrical pulses, namely the corresponding duty ratio of each leg of the new synthesized V^3 in the nine-phase OW drive system. Finally, the steady-state and dynamic performances of the proposed strategy are evaluated, in comparison to the existing V^3 with duty ratio optimization-based FCS-MPCC strategy. The main contributions of this article are as follows.

- 1) The synthesized new V^3 realizes the zero control error and improves the steady-state performance by 56%.
- 2) A switching pulse synthesis algorithm is designed for nine-phase OW drives, which can realize the online generation of symmetrical pulses.
- 3) The process of vector selection and duration calculation does not need any weighting factor and enumeration process, which reduces the computational burden by 13%.

The rest of this article is organized as follows. Section II introduces the nine-phase OW-PMSM system and the current predictive model. In Section III, the design method of basic V^3 is described in detail, which takes into account multiple harmonic subspaces (3rd, 5th, and 7th order). Section IV proposes the online V^3 synthesis strategy and the corresponding pulse generation algorithm in the OW drive. Section V verifies the effectiveness of the proposed FCS-MPCC through experiments. Finally, Section VI concludes this article.

II. NINE-PHASE OW-PMSM SYSTEM MODELING

The symmetrical nine-phase OW-PMSM drive system with nine sets of H-bridge converters is shown in Fig. 1. For the studied PMSM, the shape of the magnets has been optimized to reduce the harmonics, so the harmonic in the magnetic field in the air-gap is very small (<4%), and the influence of back-EMF odd harmonics in the PMSM can be neglected. The switching state $S_{x1}(x = a, b, \dots, i)$ is defined as the left leg state of the H-bridge, and the one with S_{x2} is the right leg state of the H-bridge. Employing the dc-link voltage (V_{dc}) and the switching

states, stator phase voltages can be obtained as

$$\begin{bmatrix} v_a \\ v_b \\ v_c \\ \vdots \\ v_i \end{bmatrix} = V_{dc} \begin{bmatrix} S_{a1} \\ S_{b1} \\ S_{c1} \\ \vdots \\ S_{i1} \end{bmatrix} - V_{dc} \begin{bmatrix} S_{a2} \\ S_{b2} \\ S_{c2} \\ \vdots \\ S_{i2} \end{bmatrix} = V_{dc} \begin{bmatrix} S_a \\ S_b \\ S_c \\ \vdots \\ S_i \end{bmatrix}. \quad (1)$$

For each phase, the switching state S_x has three level state 1, 0, and -1 , representing $+V_{dc}$, 0, and $-V_{dc}$, respectively. Therefore, there are $3^9 = 19683$ voltage vectors.

According to the amplitude invariant constraint, the extended VSD [9] is used for decoupling. The transformation matrix for the OW-PMSM is expressed as

$$\mathbf{C} = \frac{2}{9} \begin{bmatrix} 1 & \cos \gamma & \cos 2\gamma & \cdots & \cos 8\gamma \\ 0 & \sin \gamma & \sin 2\gamma & \cdots & \sin 8\gamma \\ 1 & \cos 3\gamma & \cos 6\gamma & \cdots & \cos 24\gamma \\ \vdots & \vdots & \vdots & \ddots & \vdots \\ 0 & \sin 7\gamma & \sin 14\gamma & \cdots & \sin 56\gamma \\ 1/2 & 1/2 & 1/2 & \cdots & 1/2 \end{bmatrix} \quad (2)$$

where $\gamma = 2\pi/9$. In motors with negligible back-EMF harmonics, as in this study, only the fundamental component $\alpha_1 - \beta_1$ contributes to the electromechanical energy conversion, while harmonic components $\alpha_h - \beta_h$ ($h = 3, 5, 7$) do not generate torque. Subsequently, to obtain the synchronous frame model, the Park transformation is applied as

$$\boldsymbol{\Gamma}_{dq0} = \begin{bmatrix} \cos n\theta & \sin n\theta \\ -\sin n\theta & \cos n\theta \end{bmatrix} \quad (3)$$

where θ is the electrical rotor position, and $n = 1, 3, 5, 7$ is the order of subspace. The $d - q$ voltage components in a rotating frame of each harmonic subspace can be calculated as

$$[v_{dn} \ v_{qn}]^T = \boldsymbol{\Gamma}_{dq0} [v_{\alpha n} \ v_{\beta n}]^T. \quad (4)$$

Based on (4), the stator voltage components v_{d1} and v_{q1} of the PMSM in $d_1 - q_1$ reference frame are

$$\begin{bmatrix} v_{d1} \\ v_{q1} \end{bmatrix} = \begin{bmatrix} R_s & -\omega_e L_{q1} \\ \omega_e L_{d1} & R_s \end{bmatrix} \begin{bmatrix} i_{d1} \\ i_{q1} \end{bmatrix} + \begin{bmatrix} L_{d1} \\ L_{q1} \end{bmatrix} p \begin{bmatrix} i_{d1} \\ i_{q1} \end{bmatrix} + \begin{bmatrix} 0 \\ \omega_e \psi_f \end{bmatrix}. \quad (5)$$

The $d_h - q_h$ stator voltage vector harmonic components v_{dh} and v_{qh} are given by

$$\begin{bmatrix} v_{dh} \\ v_{qh} \end{bmatrix} = \begin{bmatrix} R_s & 0 \\ 0 & R_s \end{bmatrix} \begin{bmatrix} i_{dh} \\ i_{qh} \end{bmatrix} + \begin{bmatrix} L_{dh} \\ L_{qh} \end{bmatrix} p \begin{bmatrix} i_{dh} \\ i_{qh} \end{bmatrix} \quad (6)$$

where R_s is the stator phase resistance, ψ_f is the flux established by permanent magnets, ω_e represents the rotor electrical angular speed, and L_{dn} and L_{qn} are the stator $d_n - q_n$ axes inductance.

The electromagnetic torque is expressed as

$$T_e = \frac{9}{2} n_p [\psi_f i_{q1} + (L_{d1} - L_{q1}) i_{d1} i_{q1}] \quad (7)$$

where n_p is the number of pole pairs.

For FCS-MPCC, a discrete model is needed to predict the motor behavior at the next sampling time ($k+1$). According to (5) and (6), the $d_n - q_n$ axes currents in the next step can be obtained by using the forward Euler method, namely $di/dt = (i^{k+1} - i^k)/T_s$. However, in digital implementation, the computation delay will be caused by the large computation time, which can deteriorate the control performance. A valid

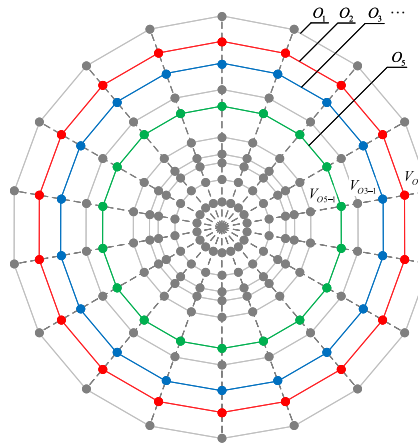


Fig. 2. Voltage vectors applicable to the nine-phase OW-PMSM drive system.

solution is using a two-step prediction to compensate the computation delay [30], where the currents at instant ($k+2$) are predicted as

$$\begin{cases} i_{d1}^{k+2} = (1 - \frac{R_s}{L_{d1}} T_s) i_{d1}^{k+1} + \frac{v_{d1}^{k+1}}{L_{d1}} T_s + T_s \omega_e^{k+1} i_{q1}^{k+1} \\ i_{q1}^{k+2} = (1 - \frac{R_s}{L_{q1}} T_s) i_{q1}^{k+1} + \frac{v_{q1}^{k+1}}{L_{q1}} T_s - T_s \omega_e^{k+1} i_{d1}^{k+1} \\ \quad - \frac{\psi_f}{L_{q1}} T_s \omega_e^{k+1} \end{cases} \quad (8a)$$

$$\begin{cases} i_{dh}^{k+2} = (1 - \frac{R_s}{L_{dh}} T_s) i_{dh}^{k+1} + \frac{v_{dh}^{k+1}}{L_{dh}} T_s \\ i_{qh}^{k+2} = (1 - \frac{R_s}{L_{qh}} T_s) i_{qh}^{k+1} + \frac{v_{qh}^{k+1}}{L_{qh}} T_s \end{cases} \quad (8b)$$

Assuming that the $\omega_e^{k+1} = \omega_e^k$ due to the negligible changing of rotor speed in consecutive control periods. After adding delay compensation, the cost function is adopted as

$$g = \sum W_n [(i_{dn}^* - i_{dn}^{k+2})^2 + (i_{qn}^* - i_{qn}^{k+2})^2] \quad (9)$$

where W_n is the weighting factor for each component and i_{dn}^* and i_{qn}^* are the reference currents. Then, the vector that minimizes the cost function is selected and output during the next control cycle.

III. BASIC V^3 S WITH ZERO HARMONIC COMPONENTS

According to [10], 181 of all voltage vectors are applicable to FCS-MPC in the nine-phase OW drive. Fig. 2 shows the 181 voltage vectors in the fundamental space $\alpha_1 - \beta_1$. They are distributed in 18 branches, each branch has 10 vectors, and the adjacent branches are separated by $\pi/9$. In order to ease the identification of vector subsets, they have been classified in ten octadecagons marked from O_1 to O_{10} in descending order of the amplitude.

Since the single vector has a fixed voltage contribution in the different subspaces, it is difficult to suppress harmonics while regulating the fundamental components [31]. According to (8b), the voltages existing in the harmonic subspaces will directly lead to low-order harmonic currents. The principle of V^3 is to use multiple single vectors to cancel each other in the harmonic subspaces, so as to nullify the average harmonic voltage production of the synthesized vector.

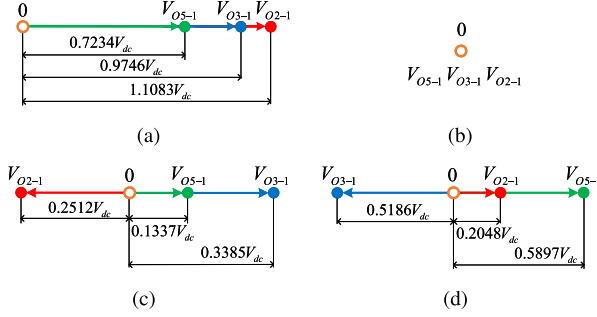


Fig. 3. Schematic of the basic V^3 synthesis. (a) $\alpha_1 - \beta_1$ subspace. (b) $\alpha_3 - \beta_3$ subspace. (c) $\alpha_5 - \beta_5$ subspace. (d) $\alpha_7 - \beta_7$ subspace.

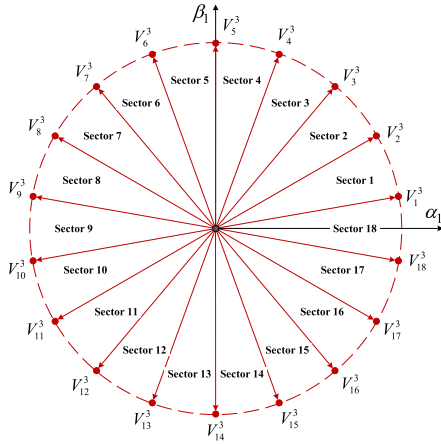


Fig. 4. Basic V^3 s and the sector definition.

In Fig. 2, the voltage vector subsets O_2 , O_3 , and O_5 can satisfy the requirement of V^3 . Taking the V_{O2-1} , V_{O3-1} , and V_{O5-1} in Fig. 2 as an example, the amplitudes in each subspace is shown in Fig. 3. In order to eliminate all the harmonics (equals zero), the dwell time of V_{O2-1} , V_{O3-1} , and V_{O5-1} in one switching cycle can be calculated as

$$\begin{bmatrix} 0 & 0 & 0 \\ -0.2512 & 0.3385 & 0.1337 \\ 0.2048 & -0.5186 & 0.5897 \end{bmatrix} \cdot \begin{bmatrix} t_{O2} \\ t_{O3} \\ t_{O5} \end{bmatrix} = \begin{bmatrix} 0 \\ 0 \\ 0 \end{bmatrix}. \quad (10)$$

It can be calculated that $t_{O2} = 0.532$, $t_{O3} = 0.347$, and $t_{O5} = 0.121$. Thus, the synthesized V^3 can be expressed as follows

$$V_m^3 = 0.532 \cdot V_{O2-m} + 0.347 \cdot V_{O3-m} + 0.121 \cdot V_{O5-m} \quad (11)$$

where $m = 1, 2, \dots, 18$. The amplitude of V^3 in $\alpha_1 - \beta_1$ is $1.015V_{dc}$. This combination mode of three vectors and the corresponding dwell times design can eliminate the low-order currents distortion, and form 18 active V^3 s, as shown in Fig. 4. The angle of V_1^3 is 10° , and the adjacent V^3 s are separated by 20° , i.e., $\pi/9$.

IV. PROPOSED ONLINE V^3 SYNTHESIS STRATEGY

Even though the V^3 -based FCS-MPCC is effective to suppress the harmonic currents, the finite and discrete vectors still limit the improvement of control performance [24]. In this section, a simple online synthesis strategy is proposed, which obtains

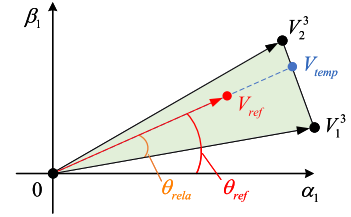


Fig. 5. Schematic of online synthesis in sector 1.

the V^3 covering the whole fundamental subspace and realizes the zero control error. Meanwhile, the symmetrical pulse sequences of each phase for the OW system are generated online to make them suitable for the implementation of the real-time system.

A. Vectors Selection

According to the positions of the basic V^3 s in Fig. 4, taking the connecting line between the V^3 s and the zero point as the boundary, the fundamental subspace is divided into 18 sectors. There are three vectors in each sector, namely two basic V^3 s and a zero vector. The vector at any point in the sector can be synthesized by the three vectors. Therefore, the vectors participating in the synthesis can be selected when the sector of the RVV is determined.

Based on the predictive model in (8a), the DBCC can be introduced to calculate the RVV in FCS-MPCC. According to the principle of deadbeat, the following constraints should be satisfied:

$$\begin{cases} i_{d1}^{k+2} = i_{d1}^* \\ i_{q1}^{k+2} = i_{q1}^* \end{cases}. \quad (12)$$

Substitute (12) into (8a), the RVV can be expressed as

$$\begin{cases} v_{d1}^* = R_s i_{d1}^{k+1} + \frac{L_{d1}}{T_s} (i_{d1}^* - i_{d1}^{k+1}) - \omega_e^{k+1} L_{q1} i_{q1}^{k+1} \\ v_{q1}^* = R_s i_{q1}^{k+1} + \frac{L_{q1}}{T_s} (i_{q1}^* - i_{q1}^{k+1}) + \omega_e^{k+1} L_{d1} i_{d1}^{k+1} + \omega_e^{k+1} \psi_f \end{cases}. \quad (13)$$

By transforming the RVV into the $\alpha_1 - \beta_1$ plane using the inverse Park transformation as follows

$$[v_{\alpha 1}^* \ v_{\beta 1}^*]^T = \Gamma_{dq1}^{-1} [v_{d1}^* \ v_{q1}^*]^T. \quad (14)$$

Subsequently, the expected RVV can be expressed in the form of a complex as

$$V_{ref} = v_{\alpha 1}^* + j v_{\beta 1}^* \quad (15)$$

where j is the imaginary unit. Hence, the phase angle of the RVV can be obtained by

$$\theta_{ref} = \arctan \left(\frac{v_{\beta 1}^*}{v_{\alpha 1}^*} \right) \cdot \frac{180^\circ}{\pi}. \quad (16)$$

According to the θ_{ref} , the sector can be determined. Taking the $\theta_{ref} = 24^\circ$ as an example, the V_{ref} is located in sector 1 ($10^\circ - 30^\circ$), and it can be synthesized by V_1^3 , V_2^3 , and the zero vector, as shown in Fig. 5.

B. Duration Ratio Calculation of Double V^3 s

Generally, the duration assignment of multiple vectors requires complex calculation and optimization process [23]–[25].

A simple calculation method is proposed in this article. As shown in Fig. 5, θ_{rela} is defined as the relative phase angle of the RVV in the located sector and calculated as follows

$$\theta_{\text{rela}} = \theta_{\text{ref}} - \varepsilon \quad (17)$$

where ε is the starting phase angle of the sector. Then, the ratio of the dwell time of the two V^3 's can be obtained as

$$\eta = \frac{\theta_{\text{rela}}}{20^\circ}. \quad (18)$$

Consequently, the temporary voltage vector V_{temp} in Fig. 5 can be expressed as

$$V_{\text{temp}} = (1 - \eta)V_m^3 + \eta V_p^3 \quad (19)$$

where $p = m + 1$, and the $m = 1$ in sector 1. By the abovementioned steps, the selection of synthesis V^3 's and the calculation of duration do not need cost function and enumeration process, which effectively reduces the computational burden and algorithm complexity.

C. Amplitude Optimization

In order to obtain a flexible amplitude regulation, the zero vector can be used for amplitude optimization of the synthetic vector. For the PMSM with control objective $i_d = 0$ in this article, the q -axis current deadbeat technique is a simple and general method to calculate the vector duty ratio [10], i.e., in C. Duty Ratio Optimization. The q -axis current predictive model can be adopted as

$$i_{q1}^{k+2} = i_{q1}^* = i_{q1}^{k+1} + s_v t_v + s_0(T_s - t_v) \quad (20)$$

where T_s is the control cycle, t_v is the dwell time of the voltage vector V_{temp} , s_v is the slope of i_{q1} when V_{temp} is applied, and s_0 is the slope of i_{q1} when the zero vector is applied. According to (8a), s_0 and s_v are derived as

$$s_0 = \frac{1}{L_{q1}}[-R_s i_{q1}^{k+1} - \omega_e^{k+1}(L_{q1} i_{d1}^{k+1} + \psi_f)] \quad (21)$$

$$s_v = s_0 + \frac{v_{q1_temp}^{k+1}}{L_{q1}} \quad (22)$$

where $v_{q1_temp}^{k+1}$ is the q -axis fundamental voltage component corresponding to V_{temp} . Thus, the optimal duty ratio can be calculated as

$$\delta = \frac{t_v}{T_s} = \frac{i_{q1}^* - i_{q1}^{k+1} - s_0 T_s}{T_s(s_v - s_0)}. \quad (23)$$

The δ should be limited within the range $0 \leq \delta \leq 1$. Finally, the synthesized new virtual vector NV^3 can be the same as the V_{ref}

$$NV^3 = \delta V_{\text{temp}} = V_{\text{ref}}. \quad (24)$$

It is worth mentioning that in MPCC, dealing with the optimal voltage vector and its optimal duration separately and simultaneously have the same results exactly [8]. Therefore, it is feasible to separate the calculation of V_{temp} and amplitude optimization in the proposed strategy.

D. New V^3 Symmetrical Pulse Generation

After obtaining NV^3 , how to generate symmetrical switching pulses is another challenge to realize online synthesis. However,

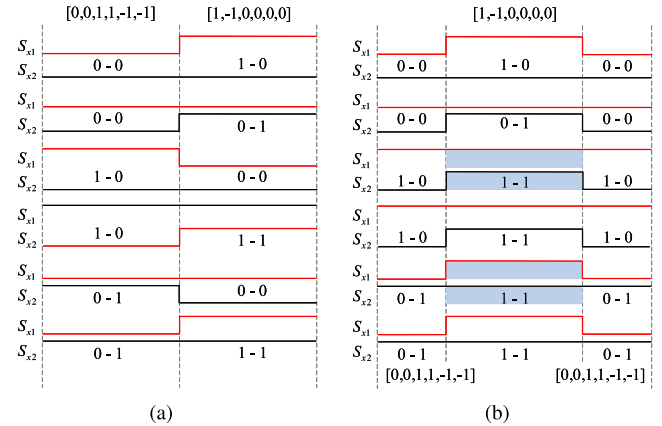


Fig. 6. Modification of the pulses in OW drive system. (a) Original pulse sequence. (b) Modified pulse sequence.

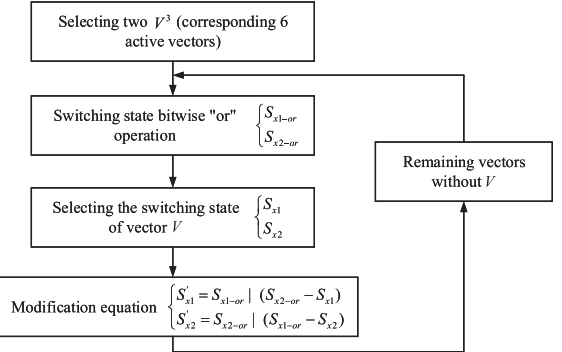


Fig. 7. Flowcharts of modifying pulse sequence.

different from the star-connected winding motor [24], [25], [31], each phase voltage in OW drive is determined by dual leg states, which output three-level effect. In addition, it is not practical to manually set the pulse sequences of all legs offline due to the complexity of multiphase systems. In order to solve this problem, an online pulse synthesis algorithm convenient for digital implementation is proposed.

According to (1), there are three switching states ($S_x = 1, 0, -1$) in the OW drive system. All the possible transitions of switching states in synthesis are shown in Fig. 6(a). It should be noted that there are two ways to obtain the state $S_x = 0$, namely $S_{x1} = S_{x2} = 0$ and $S_{x1} = S_{x2} = 1$. Utilizing this characteristic of OW drive, as shown in Fig. 6(b), the switching state can be modified to synthesize symmetrical pulses while maintaining the voltage vector unchanged. The shadow part in Fig. 6(b) is the pulse replacing 0-0 with 1-1.

Based on this principle, the flowcharts of synthesis vector pulses modification is designed as Fig. 7. Taking the V_{ref} in Fig. 5 as an example, the V_1^3 and V_2^3 are selected, which correspond to six active vectors, as shown in Fig. 8. The original switching states of the six vectors are listed in Table I. The switching states "or" operation means that S_{x1} and S_{x2} of all six vectors are calculated, respectively, with bitwise "or." The result is expressed as

$$\begin{cases} S_{x1-or} = [1, 1, 1, 0, 0, 0, 0, 1] \\ S_{x2-or} = [0, 0, 0, 1, 1, 1, 1, 0] \end{cases}. \quad (25)$$

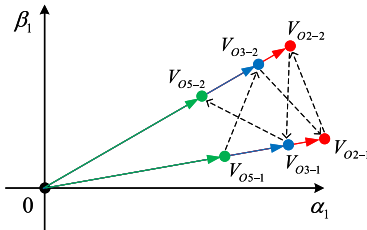


Fig. 8. Vector selection order in pulse modification.

TABLE I
ORIGINAL SWITCHING STATES OF THE SIX VECTORS IN SECTOR1

Vector	S_{x1}	S_{x2}	S_x
V_{O2-1}	[1,1,0,0,0,0,0,1]	[0,0,0,0,1,1,1,0,0]	[1,1,0,0,-1,-1,-1,0,1]
V_{O3-1}	[1,1,1,0,0,0,0,0,0]	[0,0,0,1,1,1,0,0,0]	[1,1,1,-1,-1,-1,0,0]
V_{O5-1}	[1,0,0,0,0,0,0,1]	[0,0,0,0,0,1,1,0,0]	[1,0,0,0,0,-1,-1,0,1]
V_{O2-2}	[1,1,1,0,0,0,0,0,0]	[0,0,0,0,1,1,1,0,0]	[1,1,1,0,-1,-1,-1,0,0]
V_{O3-2}	[1,1,0,0,0,0,0,1]	[0,0,0,0,0,1,1,1,0]	[1,1,0,0,0,-1,-1,-1,1]
V_{O5-2}	[0,1,1,0,0,0,0,0,0]	[0,0,0,0,1,1,0,0,0]	[0,1,1,0,-1,-1,0,0,0]
"or"	[1,1,1,0,0,0,0,1]	[0,0,0,1,1,1,1,1,0]	/

It can be seen that S_{x1-or} (S_{x2-or}) is the result of six S_{x1} (S_{x2}). Then, the vector that needs to modify the switching states is selected and replaced with the new states. The general selection order is

$$V_{O5-m} - V_{O3-p} - V_{O2-m} - V_{O2-p} - V_{O3-m} - V_{O5-p}. \quad (26)$$

In the example, the modification order is shown in Fig. 8. Start with V_{O5-1} , corresponding to the S_{x1} and S_{x2} of V_{O5-1} , the states modification equation is used to generate the alternative states

$$\left\{ \begin{array}{l} S'_{x1} = S_{x1-or} | (S_{x2-or} - S_{x2}) \\ = [1, 1, 1, 0, 0, 0, 0, 1] | [0, 0, 0, 1, 1, 0, 0, 1, 0] \\ = [1, 1, 1, 1, 0, 0, 1, 1] \\ S'_{x2} = S_{x2-or} | (S_{x1-or} - S_{x1}) \\ = [0, 0, 0, 1, 1, 1, 1, 0] | [0, 1, 1, 0, 0, 0, 0, 0, 0] \\ = [0, 1, 1, 1, 1, 1, 1, 0] \end{array} \right. \quad (27)$$

where $S_{x2-or} - S_{x2}$ is bitwise calculated as

$$\begin{aligned} S_{x2-or} - S_{x2} &= [0, 0, 0, 1, 1, 1, 1, 0] \\ &\quad - [0, 0, 0, 0, 0, 1, 1, 0, 0] \\ &= [0, 0, 0, 1, 1, 0, 0, 1, 0]. \end{aligned} \quad (28)$$

Subsequently, the remaining vectors in the six vectors are calculated again with bitwise "or," and the abovementioned process is repeated. Finally, the modified switching states are shown in Table II, where the states with bold font are different from the original states. According to (1), it can be seen that the voltage vectors (corresponding to the switching state S_x) of the OW drive system are maintained.

Based on the switching state modification, the duty cycle of legs d_{x1} and d_{x2} are expressed as

$$\begin{bmatrix} d_{x1} \\ d_{x2} \end{bmatrix} = \delta(1 - \eta) \begin{bmatrix} t_{O2} \\ t_{O3} \\ t_{O5} \end{bmatrix} \begin{bmatrix} S_{x(O2-m)} \\ S_{x(O3-m)} \\ S_{x(O5-m)} \end{bmatrix}$$

TABLE II
MODIFIED SWITCHING STATES OF THE SIX VECTORS IN SECTOR1

Vector	S'_{x1}	S'_{x2}	S_x
V_{O2-1}	[1,1,1,1,0,0,0,1]	[0,0,1,1,1,1,0,0]	[1,1,0,0,-1,-1,0,1]
V_{O3-1}	[1,1,1,0,0,0,0,0]	[0,0,0,1,1,1,0,0]	[1,1,1,-1,-1,0,0]
V_{O5-1}	[1,1,1,1,0,0,1,1]	[0,1,1,1,1,1,1,0]	[1,0,0,0,0,-1,-1,0,1]
V_{O2-2}	[1,1,1,1,0,0,0,0]	[0,0,0,1,1,1,1,0]	[1,1,1,0,-1,-1,-1,0,0]
V_{O3-2}	[1,1,1,1,1,0,0,1]	[0,0,1,1,1,1,1,0]	[1,1,0,0,0,-1,-1,-1,1]
V_{O5-2}	[0,1,1,0,0,0,0,0]	[0,0,0,0,1,1,0,0]	[0,1,1,0,-1,-1,0,0]

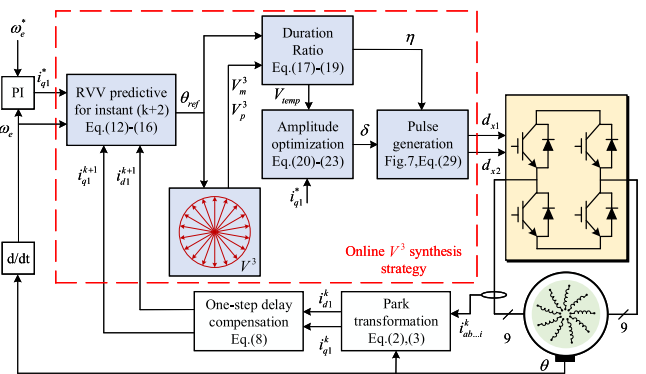


Fig. 9. Control diagram of the proposed FCS-MPC method.

$$+ \delta \eta \begin{bmatrix} t_{O2} \\ t_{O3} \\ t_{O5} \end{bmatrix} \begin{bmatrix} S_{x(O2-m)} \\ S_{x(O3-m)} \\ S_{x(O5-m)} \end{bmatrix} \quad (29)$$

where the switching states are replaced with modified states. Taking the $S_{x(O2-m)}$ as an example, the S'_{x1} and S'_{x2} of V_{O2-m} are used. Substitute Table II, $\eta = 0.7$, and $\delta = 0.8$ into (29), the symmetrical pulses duty cycle of all legs are obtained as

$$\begin{cases} d_{x1} = [0.7325, 0.8, 0.8, 0.6491, 0.2234, 0, 0, 0.0289, 0.3511] \\ d_{x2} = [0, 0.0289, 0.3511, 0.7325, 0.8, 0.8, 0.6491, 0.2234, 0] \end{cases}.$$

There is $d_{x1} - d_{x2} = NV^3$. Consequently, the predictive V_{ref} is output accurately by synthesized pulses, which eliminate the control error.

E. Overall Control Algorithm

The control diagram of the proposed FCS-MPC is depicted in Fig. 9, where the proposed online V^3 synthesis strategy is marked in the red block. Among them, the V^3 eliminates the harmonic voltage components in 3rd, 5th, and 7th subspaces. The vector selection and duration ratio calculation are simple to implement, which effectively reduce the computational burden. Moreover, the problem of online symmetrical pulse generation in OW drive system is solved and suitable for implementation of digital processors.

It should be noted that although the deadbeat principle is introduced into the proposed method, the robustness will not deteriorate obviously. This is because the voltage vector synthesized online by the proposal can cover the whole fundamental subspace, under the case of parameters mismatch, the output voltage vector will still be closer to the "correct" reference vector than the original discrete vectors.

TABLE III
MAIN CHARACTERISTICS OF MPC STRATEGIES WITH ONLINE MULTIVECTOR SYNTHESIS

	DVV [22]	SVV [23]	M ² PC [26]	Proposed
Need of weighting factors	XX	X	X	✓✓
Calculation and complexity	XX	XX	X	✓
Low switching frequency	✓✓	✓	Fixed as f_{sa}	✓
Harmonic distortion	✓	✓✓	✓✓	✓✓
Control error	✓	✓✓	✓✓	✓✓

Note: Scaled from best (✓✓) to worst (XX) and f_{sa} is the sampling frequency.

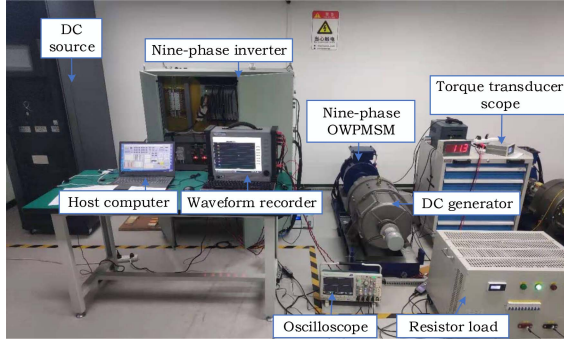


Fig. 10. Test bench.

TABLE IV
KEY PARAMETERS OF THE TEST BENCH

Specification	Value	Specification	Value
Rated motor power	9 kW	D_1 -axis inductance	41.22 mH
Rated speed	900 r/min	Q_1 -axis inductance	41.22 mH
Rated torque	95.5 N·m	Stator resistance	2.47 Ω
Rated current (rms)	4.6 A	Permanent magnet flux	0.8524 Wb
Number of pole pairs	4	DC-link voltage	450 V

Compared to other papers on the topic [22], [23], [26], the proposed method applies V^3 's to achieve harmonic currents suppression without weighting factors. The two optimal V^3 's are selected by the predicted RVV without the cost function. The duration of each V^3 and the zero vector is calculated by simple analytical expressions without searching discrete points. Moreover, a switching pulse synthesis algorithm has been designed to generate the symmetrical pulses of the multiphase H-bridges converters. Finally, Table III summarizes the main characteristics of the relevant MPC strategies.

V. EXPERIMENTAL RESULTS

A. Test Bench

To verify the effectiveness of the proposed strategy in the nine-phase OW-PMSM system, a 9 kW experimental prototype is established, as shown in Fig. 10. The main parameters of the test bench are depicted in Table IV. The symmetrical nine-phase OW-PMSM is powered by nine H-bridges with intelligent power modules (Mitsubishi PM75RLA120). The output phase currents are measured with LA55-P current sensors. The controller is composed of TMS320F28335 (for digital calculation) and Xilinx-xc4 (for sampling, protection, and pulse output), and they are connected by the external interface (XINTF).

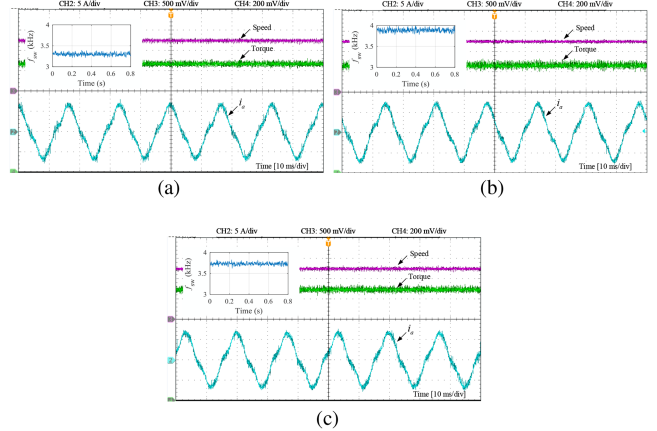


Fig. 11. Experimental results of the steady-state underrated operation. (a) FCS-MPCC-I with $f_{sa} = 5$ kHz. (b) FCS-MPCC-I with $f_{sa} = 6$ kHz. (c) FCS-MPCC-II with $f_{sa} = 5$ kHz.

The nine-phase OW-PMSM is loaded with the shaft connected to a dc machine that acts as a generator. The armature of the dc machine is connected to a variable passive resistance load that dissipates the power, and the load torque is consequently speed dependent.

For simplicity, the existing V^3 with amplitude (duty cycle) optimization-based FCS-MPCC is termed as FCS-MPCC-I, which uses basic V^3 's in Fig. 4 as the control set. The proposed online V^3 synthesis strategy is termed as FCS-MPCC-II. The sampling time is set as 200 μ s (5 kHz) in the control platform. Meanwhile, in order to verify the control performance at a similar switching frequency (f_{sw}), the sampling frequency (f_{sa}) of FCS-MPCC-I is also set as 166.67 μ s (6 kHz) for testing.

B. Steady-State Performance

Fig. 11 compares the steady-state phase current performance of the two FCS-MPCCs mentioned above with a rated load and speed. It can be seen that both methods can realize stable operation, and the phase currents performance are similar. To compare switching frequencies, the average f_{sw} is computed by

$$f_{sw} = \frac{1}{18T_w} \sum_{x=a}^i \sum_{y=1}^2 N_{xy} \quad (30)$$

where T_w is the time window in which the ON-OFF times of IGBTs are counted, and T_w is set to 0.1 s in this test. N_{xy} represents the ON-OFF times of leg xy ($x = a, b, \dots, i$; $y = 1, 2$). When the f_{sa} is 5 kHz, the f_{sw} of FCS-MPCC-II (3.75 kHz) is 13% higher than that of FCS-MPCC-I (3.31 kHz). This is because FCS-MPCC-I uses three active switching states plus one zero vector in the synthesized virtual vector, while FCS-MPCC-II uses six active switching states plus one zero vector. It should be noted that, although the active switching state in FCS-MPCC-II is twice as that of the FCS-MPCC-I, the f_{sw} of FCS-MPCC-II only increases slightly (13%). This is because the switching states added in FCS-MPCC-II only causes a few additional legs to generate switching action.

In order to compare more fairly, the f_{sa} of FCS-MPCC-I is increased to 6 kHz. The steady-state results under rated operation

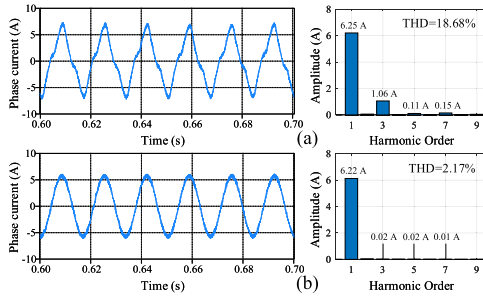


Fig. 12. Simulation results of the evaluation of dead-time effects in FCS-MPCC-II. (a) Dead-time is $3 \mu\text{s}$. (b) No dead-time.

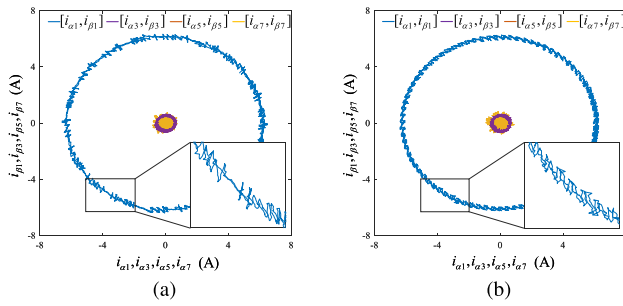


Fig. 13. Steady-state current trajectories in $\alpha_n - \beta_n$ subspace. (a) FCS-MPCC-I with $f_{sa} = 6 \text{ kHz}$. (b) FCS-MPCC-II with $f_{sa} = 5 \text{ kHz}$.

is shown in Fig. 11(b). In this case, the f_{sw} is 3.94 kHz, which is slightly higher than that of FCS-MPCC-II (3.75 kHz). The total harmonic distortion (THD) for the FCS-MPCC-I and FCS-MPCC-II schemes are 13.31% and 14.77%, respectively. The remaining harmonic current is mainly the 3rd, although the 3rd harmonic voltage in V^3 is zero. This is caused by the intrinsic dead-time effects, which can be proved by the simulation results. In Fig. 12(a), the dead-time is set to $3 \mu\text{s}$, the same as that of in the experiment. It can be seen that the phase current contains 3rd harmonic current, which is the main reason for the increase of THD. It is consistent with the experimental waveform in Fig. 11. This is because the largest voltage harmonic generated by the dead-time is the 3rd, which is mapped on the harmonic subspace with very low impedance, leading to a potentially 3rd harmonic current flow [3]. In contrast, when the dead-time is removed (only can be realized in simulation), as shown in Fig. 12(b), the phase current becomes very sinusoidal, and the THD is only 2.17%. Therefore, it can be concluded that the dead-time effect is the cause of the remaining harmonic currents.

The current trajectories in $\alpha_1 - \beta_1$ and $\alpha_h - \beta_h$ subspaces are shown in Fig. 13. It is clear that the fundamental current of the FCS-MPCC-II is more stable than that in FCS-MPCC-I, and the harmonic currents are effectively suppressed.

Fig. 14(a) shows the results of electromagnetic torque T_e , which is calculated by (7). The standard deviation (SD) is used in this article to quantify the ripple. Obviously, the proposed FCS-MPCC-II can provide more stable torque output. Furthermore, the duty cycle δ in amplitude optimization is compared by Fig. 14(b). For basic V^3 -based FCS-MPCC-I, even though the duty cycle can reduce the error between the output vector and the RVV, this control error cannot be completely eliminated. In addition, the error is always excess corrected because the

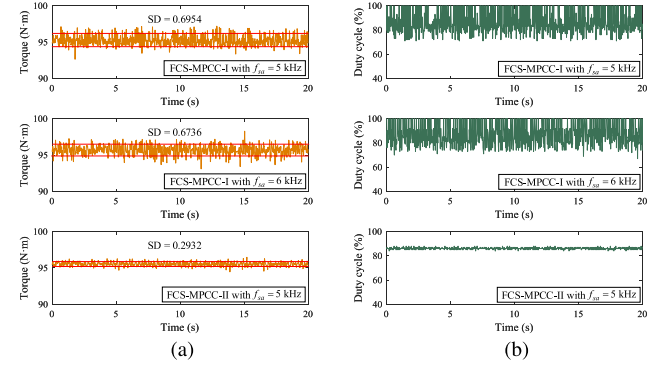


Fig. 14. Experimental results of the electromagnetic torque and duty cycle. (a) Torque waveform. (b) Duty cycle waveform.

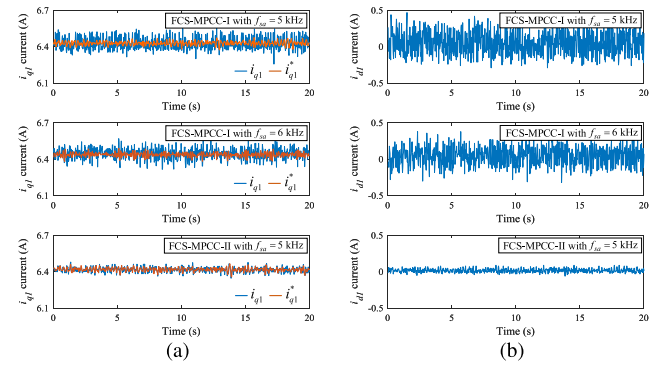


Fig. 15. Experimental results of the fundamental current components. (a) i_{q1} current waveform. (b) i_{d1} current waveform.

TABLE V
COMPARISON OF THE STUDIED METHODS AT SAME SAMPLING FREQUENCY AND SIMILAR AVERAGE SWITCHING FREQUENCY

Control Schemes	FCS-MPCC-I	FCS-MPCC-II
f_{sa}	5 kHz	6 kHz
f_{sw}	3.31 kHz	3.94 kHz
T_e SD	0.6954	0.6736
i_{q1} SD	0.0475	0.0436
i_{d1} SD	0.1553	0.1282

phase angle of the output vector is finite. Therefore, the δ in FCS-MPCC-I presents a sharp fluctuation. Comparatively, the δ in FCS-MPCC-II is stable because the amplitude and phase angle of the synthesized V^3 in each control cycle can accurately reach the RVV.

The experimental results in Fig. 15 proved the improvement of FCS-MPCC-II on steady-state performance. This article uses $i_d = 0$ control. There are substantial ripple currents caused by control error in FCS-MPCC-I. In comparison, the feedbacks of i_{d1} and i_{q1} in FCS-MPCC-II almost coincide with the reference value due to the zero control error. Comparison of the two methods at the same sampling frequency and similar average switching frequency is summarized in Table V. It can be observed that under the same/similar average switching frequency, the proposed method can still reduce the torque ripple by 56%, compared to FCS-MPCC-I.

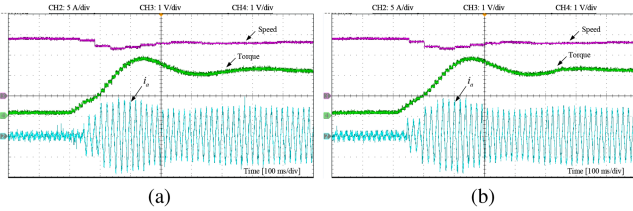


Fig. 16. Experimental results of rated load step change response. (a) FCS-MPCC-I with $f_{sa} = 6$ kHz. (b) FCS-MPCC-II with $f_{sa} = 5$ kHz.

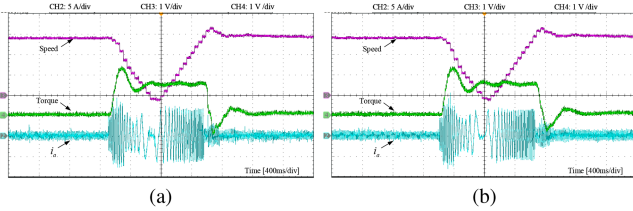


Fig. 17. Experimental results of speed reversal response. (a) FCS-MPCC-I with $f_{sa} = 6$ kHz. (b) FCS-MPCC-II with $f_{sa} = 5$ kHz.

In addition, the execution time for the FCS-MPCC-I and FCS-MPCC-II schemes are 96 μ s and 83 μ s, respectively. The computational burden is effectively reduced by 13% in FCS-MPCC-II, even the vector online synthesis is realized.

C. Dynamic Performance

In order to evaluate the dynamic performance of the proposed scheme, two methods are tested under the similar f_{sw} . Fig. 16 shows the results of load step change response. The load torque steps up from zero to rated value (95.5 N·m) under the maximum speed of 900 r/min. It can be observed that the rotor speed returns to its reference value quickly after the load step change moment with both control schemes, which have a similar load disturbance response.

Fig. 17 demonstrates the dynamic performance of speed reversal response. The PMSM was running first at negative rated speed (-900 r/min) then the speed is reversed to positive rated speed (900 r/min). The speed waveform is showing the absolute value from the output of the speed transducer. It can be concluded that both methods can satisfactorily achieve fast response and low overshoot for the speed tracking.

To sum up, the proposed online V^3 synthesis-based FCS-MPCC strategy can be successfully applied to the nine-phase OW-PMSM system. The experimental results show that the current tracking and torque ripple are significantly improved compared with the existing V^3 with amplitude optimization-based FCS-MPCC strategy.

VI. CONCLUSION

In this article, an online V^3 synthesis strategy was proposed to address the control error caused by voltage vector discretization in traditional FCS-MPCC. Using two basic V^3 's without harmonic components and a zero vector to synthesize, a new V^3 was able to cover the whole fundamental subspace. The proposed vector selection and duration ratio calculation did not need enumeration and optimization process, which effectively reduced the computational burden. In addition, an online symmetrical

pulse synthesis algorithm was designed to solve the pulse generation problem of multivector synthesis in the nine-phase OW drive system. By the proposed strategy, the steady-state performance of the system was significantly improved. In comparison to the existing FCS-MPCC strategy, the torque ripple was suppressed by 56%. Besides, the computational effort was also reduced by 13% compared with the conventional virtual vector technique. Although this article concentrated on the nine-phase OW-PMSM drive, the proposed online synthesis strategy can also be extended to other MPC-based multiphase OW drives.

REFERENCES

- [1] S. Rubino, O. Dordevic, R. Bojoi, and E. Levi, "Modular vector control of multi-three-phase permanent magnet synchronous motors," *IEEE Trans. Ind. Electron.*, vol. 68, no. 10, pp. 9136–9147, Oct. 2021.
- [2] M. J. Duran and F. Barrero, "Recent advances in the design, modeling, and control of multiphase machines-Part II," *IEEE Trans. Ind. Electron.*, vol. 63, no. 1, pp. 449–458, Jan. 2016.
- [3] E. Levi, "Advances in converter control and innovative exploitation of additional degrees of freedom for multiphase machines," *IEEE Trans. Ind. Electron.*, vol. 63, no. 1, pp. 433–448, Jan. 2016.
- [4] F. Yu, S. Zhao, Z. Tian, and X. Wu, "Model predictive flux control of semicontralled open-winding PMSG with circulating current elimination," *IEEE Trans. Ind. Informat.*, vol. 17, no. 2, pp. 1438–1448, Feb. 2021.
- [5] J. Rodriguez *et al.*, "Latest advances of model predictive control in electrical drives-Part I: Basic concepts and advanced strategies," *IEEE Trans. Power Electron.*, vol. 37, no. 4, pp. 3927–3942, Apr. 2022.
- [6] P. Garcia-Entrambasaguas, I. Zoric, I. González-Prieto, M. J. Duran, and E. Levi, "Direct torque and predictive control strategies in nine-phase electric drives using virtual voltage vectors," *IEEE Trans. Power Electron.*, vol. 34, no. 12, pp. 12106–12119, Dec. 2019.
- [7] M. Bermudez, M. R. Arahal, M. J. Duran, and I. González-Prieto, "Model predictive control of six-phase electric drives including ARX disturbance estimator," *IEEE Trans. Ind. Electron.*, vol. 68, no. 1, pp. 81–91, Jan. 2021.
- [8] Y. Zhang, D. Xu, J. Liu, S. Gao, and W. Xu, "Performance improvement of model-predictive current control of permanent magnet synchronous motor drives," *IEEE Trans. Ind. Appl.*, vol. 53, no. 4, pp. 3683–3695, Jul./Aug. 2017.
- [9] M. Cheng, F. Yu, K. T. Chau, and W. Hua, "Dynamic performance evaluation of a nine-phase flux-switching permanent-magnet motor drive with model predictive control," *IEEE Trans. Ind. Electron.*, vol. 63, no. 7, pp. 4539–4549, Jul. 2016.
- [10] H. Wang, X. Wu, X. Zheng, and X. Yuan, "Virtual voltage vector based model predictive control for a nine-phase open-end winding PMSM with a common DC bus," *IEEE Trans. Ind. Electron.*, vol. 69, no. 6, pp. 5386–5397, Jun. 2022.
- [11] C. Xue, W. Song, and X. Feng, "Finite control-set model predictive current control of five-phase permanent-magnet synchronous machine based on virtual voltage vectors," *IET Electr. Power Appl.*, vol. 11, no. 5, pp. 836–846, May 2017.
- [12] I. González-Prieto, M. J. Duran, J. J. Aciego, C. Martin, and F. Barrero, "Model predictive control of six-phase induction motor drives using virtual voltage vectors," *IEEE Trans. Ind. Electron.*, vol. 65, no. 1, pp. 27–37, Jan. 2018.
- [13] W. Hua, F. Chen, W. Huang, G. Zhang, W. Wang, and W. Xia, "Multivector-based model predictive control with geometric solution of a five-phase flux-switching permanent magnet motor," *IEEE Trans. Ind. Electron.*, vol. 67, no. 12, pp. 10035–10045, Dec. 2020.
- [14] C. Xiong, H. Xu, T. Guan, and P. Zhou, "A constant switching frequency multiple-vector-based model predictive current control of five-phase PMSM with nonsinusoidal back EMF," *IEEE Trans. Ind. Electron.*, vol. 67, no. 3, pp. 1695–1707, Mar. 2020.
- [15] P. F. C. Gonçalves, S. M. A. Cruz, and A. M. S. Mendes, "Multistage predictive current control based on virtual vectors for the reduction of current harmonics in six-phase PMSMs," *IEEE Trans. Energy Convers.*, vol. 36, no. 2, pp. 1368–1377, Jun. 2021.
- [16] Z. Song and F. Zhou, "Observer-based predictive vector-resonant current control of permanent magnet synchronous machines," *IEEE Trans. Power Electron.*, vol. 34, no. 6, pp. 5969–5980, Jun. 2019.

- [17] C. Xue, W. Song, X. Wu, and X. Feng, "A constant switching frequency finite-control-set predictive current control scheme of a five-phase inverter with duty-ratio optimization," *IEEE Trans. Power Electron.*, vol. 33, no. 4, pp. 3583–3594, Apr. 2018.
- [18] M. S. R. Saeed, W. Song, B. Yu, and X. Wu, "Low-complexity deadbeat model predictive current control with duty ratio for five-phase PMSM drives," *IEEE Trans. Power Electron.*, vol. 35, no. 11, pp. 12085–12099, Nov. 2020.
- [19] J. Rodas, I. G. Prieto, Y. Kali, M. Saad, and J. Doval-Gandoy, "Recent advances in model predictive and sliding mode current control techniques of multiphase induction machines," *Front. Energy Res.*, vol. 9, pp. 445–466, Aug. 2021.
- [20] S.-W. Kang, J.-H. Soh, and R.-Y. Kim, "Symmetrical three-vector-based model predictive control with deadbeat solution for IPMSM in rotating reference frame," *IEEE Trans. Ind. Electron.*, vol. 67, no. 1, pp. 159–168, Jan. 2020.
- [21] T. Tao, W. Zhao, Y. He, J. Zhu, H. Tan, and R. Xue, "Multivector predictive current control for five-phase PM motor by using hybrid duty modulation technology," *IEEE Trans. Transport. Electricif.*, vol. 6, no. 4, pp. 1603–1612, Dec. 2020.
- [22] J. J. Aciego, I. González-Prieto, M. J. Duran, M. Bermudez, and P. Salas-Biedma, "Model predictive control based on dynamic voltage vectors for six-phase induction machines," *IEEE J. Emerg. Selec. Topics Power Electron.*, vol. 9, no. 3, pp. 2710–2722, Jun. 2021.
- [23] A. González-Prieto, I. González-Prieto, and M. J. Duran, "Smart voltage vectors for model predictive control of six-phase electric drives," *IEEE Trans. Ind. Electron.*, vol. 68, no. 10, pp. 9024–9035, Oct. 2021.
- [24] W. Zhao, T. Tao, J. Zhu, H. Tan, and Y. Du, "A novel finite-control-set model predictive current control for five-phase PM motor with continued modulation," *IEEE Trans. Power Electron.*, vol. 35, no. 7, pp. 7261–7270, Jul. 2020.
- [25] W. Song, C. Xue, X. Wu, and B. Yu, "Modulated finite-control-set model predictive current control for five-phase voltage-source inverter," *IEEE Trans. Transport. Electricif.*, vol. 7, no. 2, pp. 718–729, Jun. 2021.
- [26] M. Ayala, J. Doval-Gandoy, J. Rodas, O. González, R. Gregor, and M. Rivera, "A novel modulated model predictive control applied to six-phase induction motor drives," *IEEE Trans. Ind. Electron.*, vol. 68, no. 5, pp. 3672–3682, May 2021.
- [27] Y. Du, J. Ji, W. Zhao, T. Tao, and D. Xu, "Self-adapted model predictive current control for five-phase open-end winding PMSM with reduced switching loss," *IEEE Trans. Power Electron.*, to be published, doi: [10.1109/TPEL.2022.3167249](https://doi.org/10.1109/TPEL.2022.3167249).
- [28] O. González *et al.*, "Model predictive current control of six-phase induction motor drives using virtual vectors and space vector modulation," *IEEE Trans. Power Electron.*, vol. 37, no. 7, pp. 7617–7628, Jul. 2022.
- [29] M. Ayala, J. Doval-Gandoy, O. González, J. Rodas, R. Gregor, and M. Rivera, "Experimental stability study of modulated model predictive current controllers applied to six-phase induction motor drives," *IEEE Trans. Power Electron.*, vol. 36, no. 11, pp. 13275–13284, Nov. 2021.
- [30] Y. Luo and C. Liu, "Elimination of harmonic currents using a reference voltage vector based-model predictive control for a six-phase PMSM motor," *IEEE Trans. Power Electron.*, vol. 34, no. 7, pp. 6960–6972, Jul. 2019.
- [31] Y. Luo and C. Liu, "Multi-vector-based model predictive torque control for a six-phase PMSM motor with fixed switching frequency," *IEEE Trans. Energy Convers.*, vol. 34, no. 3, pp. 1369–1379, Sep. 2019.



Haifeng Wang (Graduate Student Member, IEEE) was born in Taian, China, in 1992. He received the B.S. degree in electrical engineering from the Harbin University of Science and Technology, Weihai, China, in 2015, and the M.S. degree in electrical engineering in 2018 from Qingdao University, Qingdao, China, where he is currently working toward the Ph.D. degree in electrical engineering.

His current research interests include multiphase electric machine drives and model predictive control.



Xinzhen Wu received the B.S. degree from Tsinghua University, Beijing, China, in 1986, the M.S. degree from Southeast University, Nanjing, China, in 1989, and the Ph.D. degree from Tsinghua University, in 2006, all in electrical engineering.

He became an Assistant Professor in 1992, an Associate Professor in 1996, and a Full Professor of Electrical Engineering in 2000 with Qingdao University, Qingdao, China. He has authored or coauthored more than 100 technical papers. His research interests include design, analysis, and control of multiphase electric machines and their systems.

Prof. Wu is currently the Principal Investigator of the Key Project of National Natural Science Foundation of China.



Xiaoqin Zheng (Member, IEEE) received the B.S. degree in automation from Linyi University, Linyi, China, in 2008, the M.S. degree in electrical engineering from Qingdao University, Qingdao, China, in 2012, and the Ph.D. degree in electrical engineering from the Huazhong University of Science and Technology, Wuhan, China, in 2017.

Since 2017, she has been with Qingdao University, where she is currently an Associate Professor with the College of Electrical Engineering. Her main research interests include performance analysis and fault-tolerant control of multiphase machines.



Xibo Yuan (Senior Member, IEEE) received the B.S. degree from the China University of Mining and Technology, Xuzhou, China, in 2005, and the Ph.D. degree from Tsinghua University, Beijing, China, in 2010, both in electrical engineering.

Since 2017, he has been a Professor with the University of Bristol, Bristol, U.K. His research interests include power electronics and motor drives, wind power generation, multilevel converters, application of wide-bandgap devices, electric vehicles, and more electric aircraft technologies.

Prof. Yuan is currently an Associate Editor for the IEEE TRANSACTIONS ON INDUSTRY APPLICATIONS and IEEE JOURNAL OF EMERGING AND SELECTED TOPICS IN POWER ELECTRONICS. He is a Fellow of IET. He was the recipient of The Isao Takahashi Power Electronics Award in 2018.